Journal of Solid State Chemistry **145,** 227–234 (1999)
Article ID jssc.1999.8252, available online at http://www.idealibrary.com on IDEAL®

Synthesis of New Network Phosphates with NZP Structure

G. Buvaneswari and U. V. Varadaraju

Material Science Research Centre, Indian Institute of Technology, Chennai-36, India

Received December 7, 1998, in revised form February 22, 1999; accepted February 26, 1999

New NZP-type phosphates of the formula $PbM^{3+}M^{4+}P_3O_{12}$ (M^{3+} = Cr, Fe, and In; M^{4+} = Ti, Zr, Hf, and Sn) were synthesized. The evolution of lattice parameters with radii of M^{3+} and M^{4+} cations indicates the anomalous behavior of tin-containing compounds. The room temperature structure of $PbFeZrP_3O_{12}$ has been refined using powder neutron diffraction data. The compounds were characterized by infrared and electronic spectroscopic methods. $Pb_{0.5}Mo_2P_3O_{12}$ with molybdenum present in the reduced state (+4) was synthesized. It is found that $Pb_{0.5}Mo_2P_3O_{12}$ is structurally related to $TlMo_2P_3O_{12}$ and crystallizes in an orthorhombic system with parameters a = 8.621 Å; b = 9.492 Å; c = 12.486 Å. © 1999 Academic Press

***Key Words*: NZP; orthophosphates; neutron diffraction.**

INTRODUCTION

Open framework phosphates of the general formula $AM_2P_3O_{12}$, crystallizing in the NZP ($NaZr_2P_3O_{12}$) structure, are important in view of their fast-ion conduction and low thermal expansion behaviour (1, 2). The compounds are also studied for redox insertion and extraction reactions (3–6), for ion-exchange reactions (7), and for the immobilization of radioactive nuclides (8). These characteristic properties are attributed to the unique crystal structure of NZP.

The crystal structure of the prototype composition $NaZr_2P_3O_{12}$ was first reported by Hagman and Kierkegaard (9). It has rhombohedral symmetry with $R\bar{3}C$ space group and the equivalent hexagonal unit cell has dimensions $a = 8.804$ Å and $c = 22.758$ Å. The basic structure consists of a framework of corner shared PO_4 tetrahedra and ZrO_6 octahedra. This polyhedral interconnection gives rise to two types of interstitial sites with distinct geometries. The site with a distorted octahedral coordination of oxygen is referred to as the type I site and that with trigonal prismatic coordination is referred to as the type II site. The type I sites (6*b*) are situated between two ZrO_6 octahedra along the axis of the $O_3ZrO_3(PO_4)_3O_3ZrO_3$ ribbons (*c*-axis) and the type II sites (18*e*) are located between these ribbons. These vacant sites are interconnected to form 3D tunnels through which the charge compensating *A*-cations can diffuse.

An interesting aspect of the crytal chemistry of the NZP structure is its extraordinary flexibility toward cationic substitutions at different lattice sites leading to numerous chemical compositions. There are also compounds with vacant interstitial sites (e.g., $M^{5+}Ti^{4+}P_3O_{12}$) (10). The flexibility of the framework is further demonstrated by the existence of compounds with H^+, the smallest ion, and Cs^+, one of the largest ions at the *A* site (11, 12). By suitable charge compensating substitutions at the Zr site, compounds with divalent and higher valent ions occupying the type I site can also be synthesized (13–16). Thus, the NZP frame work is ideal for developing a suitable composition that can meet the desired requirements for a specific application.

The present work reports on the synthesis of a series of new compounds of the formula $Pb^{2+}M^{3+}M^{4+}P_3O_{12}$ (M^{3+} = Cr, Fe and In; M^{4+} = Ti, Zr, Hf, and Sn) and stabilization of elements with lower oxidation states (Ti^{3+} and Mo^{4+}) in the orthophosphate lattice, e.g., $Pb^{+2}Ti^{+3}Ti^{+4}P_3O_{12}$ and $Pb^{2+}_{0.5}Mo^{4+}_2P_3O_{12}$. The structural features of the compound $PbFeZrP_3O_{12}$ are determined by the Rietveld profile refinement of the powder neutron diffraction pattern. Since the properties such as thermal expansion and ionic conductivity depend on the nature of the ions present in the vacant sites, it is interesting to synthesize and study this NZP family of compounds with bulky Pb^{2+} ion.

EXPERIMENTAL

Synthesis

The compounds were synthesized by high temperature solid state reaction from high pure PbO, Cr_2O_3, Fe_2O_3, In_2O_3, TiO_2, ZrO_2, HfO_2, SnO_2, and $NH_4H_2PO_4$. Stoichiometric mixtures of the metal oxides and ammonium dihydrogen phosphate were heated in air at 300°C for 6 h to eliminate H_2O and NH_3. The resultant mixture was heated in the powder form at 600°C for 12 h and at 900°C for 24 h with intermittent grindings. The powder samples were pelletized and sintered in the range of temperature from 1050

0022-4596/99 $30.00

to 1200°C depending on the nature of the M^{3+} and M^{4+} ions present in the composition.

The compounds $Pb^{+2}Ti^{+3}Ti^{+4}P_3O_{12}$ and $Pb_{0.5}Mo_2P_3O_{12}$ were synthesized by solid state reduction of Ti^{4+} and Mo^{6+} by Ti and Mo metal powders (17, 18). In the first step an off-stoichiometric mixture of PbO, TiO_2/MoO_3, and $NH_4H_2PO_4$ was heated in air at 300°C for 6 h and at 600°C for 12 h. This treatment removes all the volatiles and enables further reaction in an evacuated sealed quartz tube. In the second step, the resulting "master composition" was thoroughly mixed with the required amount of Ti or Mo metal powder. The mixture was pelletized and the pellets were heat treated at 900°C in an evacuated ($\sim 10^{-5}$ torr) and sealed quartz tube for 24 h. The pellets were ground well, repelletized, and heated in sealed quartz tubes at 900°C for 24 h with intermittent grinding to ensure the homogeneity of the mixture. Finally the pellets of Ti-containing compound were sintered at 1050°C for 24 h and those of Mo-containing compound at 1000°C for 24 h in evacuated and sealed quartz tubes. The reaction scheme is given below:

1. $PbO + 1.75TiO_2 + 3NH_4H_2PO_4 \xrightarrow[\text{air}]{\Delta}$ Master composition $+ H_2O + NH_3\uparrow$

   Master composition $+ 0.25$ Ti $\xrightarrow[\text{vacuum}]{\Delta} Pb^{+2}Ti^{+3}Ti^{+4}P_3O_{12}$

2. $0.5\ PbO + 1.3333\ MoO_3 + 3NH_4H_2PO_4 \xrightarrow[\text{air}]{\Delta}$ Master composition $+ H_2O + NH_3\uparrow$

   Master composition $+ 0.6667$ Mo $\xrightarrow[\text{vacuum}]{\Delta} Pb_{0.5}Mo_2P_3O_{12}$.

The formation process was monitored for the compound $PbFeZrP_3O_{12}$ by recording XRD patterns at RT of the reactant mixture heated at various temperatures as mentioned above. The elimination of water and ammonia at 300°C left behind a mixture of oxides (PbO, Fe_2O_3, and ZrO_2) and other amorphous phases. Heating at 600°C resulted in the formation of phosphates such as PbP_2O_6, $Pb_2P_2O_7$, $FePO_4$, $Zr(PO_3)_4$, and α-$Zr_2P_2O_9$. At 900°C all the lower phosphates decomposed and the formation of $PbFeZrP_3O_{12}$ together with ZrP_2O_7 was noted. Heating at 1100°C eliminated the ZrP_2O_7 phase and resulted in single phase formation of $PbFeZrP_3O_{12}$.

Characterization

The compounds were characterized by powder X-ray diffraction (Rich Seifert, Germany, Cu$K\alpha_1$) at room temperature. Potassium chloride was used as an internal standard. The diffraction patterns were indexed by using the LAZY PULVERIX program. The lattice parameters were obtained by LSQ fitting of high angle reflections. A thermal stability study was done on the mixed valent compound using Stanton Redcroft (UK) simultaneous thermal analyser STA 781 series in N_2 atmosphere in the temperature range 30–800°C using alumina as the reference material at a heating rate of 10° C/min.

The neutron powder diffraction data were collected using 1.4882 Å neutrons with the sample contained in thin-walled vanadium cans. The diffraction pattern was recorded using a position sensitive detector over the 2θ range 5.40°–105.35° in 0.05 steps.

The infrared spectra were recorded in the range 1700–400 cm^{-1} (Perkin Elmer 983) using the KBr disk technique. Diffuse reflectance spectra on select samples were recorded using a Varian Cary 2300 spectrophotometer.

RESULTS AND DISCUSSION

Phase Formation, Structure, and Stability

Phases of the formula $Pb^{2+}M^{3+}M^{4+}P_3O_{12}$ (M^{3+} = Cr, Fe and In; M^{4+} = Ti, Sn, Hf, and Zr), $Pb^{+2}Ti^{+3}Ti^{+4}P_3O_{12}$, and $Pb_{0.5}Mo_2P_3O_{12}$ were synthesized. All the compounds show good crystallinity. In the preparation of mixed valent titanium- and molybdenum-containing compounds no reduction of Pb^{2+} either by Ti metal powder or by Mo metal powder was observed. Depending on the nature of the M^{3+} and M^{4+} ions the color of the compounds varies from white to black (Table 1).

All phases are stable toward exposure to air and moisture at room temperature. The compounds $Pb^{+2}Ti^{+3}Ti^{+4}P_3O_{12}$ and $Pb_{0.5}Mo_2P_3O_{12}$ are stable under normal conditions. Thermal analysis of $Pb^{+2}Ti^{+3}Ti^{+4}P_3O_{12}$ in N_2 atmosphere shows that the compound is stable in the temperature range 30–900°C. However, on heating in air above 500°C, the compound decomposes with consequent decoloration. The formation of TiO_2, PbO_2, and TiP_2O_7 was observed on heating the sample at 900°C and this has been confirmed by XRD.

X-ray diffraction patterns of representative members are given in Fig. 1. Figure 2 shows the pattern for $Pb_{0.5}Mo_2P_3O_{12}$. All $Pb^{2+}M^{3+}M^{4+}P_3O_{12}$ compounds are isostructural with the alkaline earth analogues (13, 19). On the other hand the XRD pattern of $Pb_{0.5}Mo_2P_3O_{12}$ shows

TABLE 1
Hexagonal Lattice Parameters of $PbM^{3+}M^{4+}P_3O_{12}$ Compounds

Compounds	Color	Lattice parameters (Å)		Volume (Å^3)
		a	*c*	
$PbTiTiP_3O_{12}$	Black	8.474	22.76	1415
$PbInTiP_3O_{12}$	White	8.513	23.09	1449
$PbCrSnP_3O_{12}$	Green	8.320	23.03	1380
$PbFeSnP_3O_{12}$	White	8.367	23.12	1402
$PbInSnP_3O_{12}$	White	8.437	23.48	1447
$PbCrHfP_3O_{12}$	Green	8.541	23.10	1459
$PbFeHfP_3O_{12}$	White	8.608	23.19	1488
$PbInHfP_3O_{12}$	White	8.710	23.50	1544
$PbCrZrP_3O_{12}$	Green	8.557	23.13	1467
$PbFeZrP_3O_{12}$	White	8.620	23.21	1494
$PbInZrP_3O_{12}$	White	8.720	23.51	1548

a strong resemblance to that of $TlMo_2P_3O_{12}$ (18). Accordingly, the pattern is indexed on the basis of an orthorhombic cell with the space group *P bcm*. The lattice parameters are $a = 8.621$ Å, $b = 9.492$ Å, and $c = 12.486$ Å. The orthorhombic structure of $TlMo_2P_3O_{12}$ is built up of corner-shared MoO_6 octahedra and PO_4 tetrahedra which form tunnels running along the *b* axis and cages, where the Tl^+ ions are located.

The XRD patterns of $Pb^{2+}M^{3+}M^{4+}P_3O_{12}$ compounds are indexed on the basis of a rhombohedral system with the space group ($R\bar{3}C$). The equivalent hexagonal parameters and the unit cell volumes are given in Table 1. It is noted that the presence of Pb^{2+} with a lone pair of $6s^2$ electrons does not cause any modification on the symmetry of the structure. Similarly the variation in the sizes of the M^{+3} and M^{+4} ions also has no effect on the structural symmetry of these phases. The cell volumes, however, are large in comparison to the alkaline earth analogues. This could be due to the stereochemical activity (20) of the $6s^2$ lone pair of the Pb^{2+} ion. Results obtained from the powder XRD study confirm that the compounds ($Pb^{2+}M^{3+}M^{4+}P_3O_{12}$) crystallize in rhombohedral symmetry, adopting the NZP

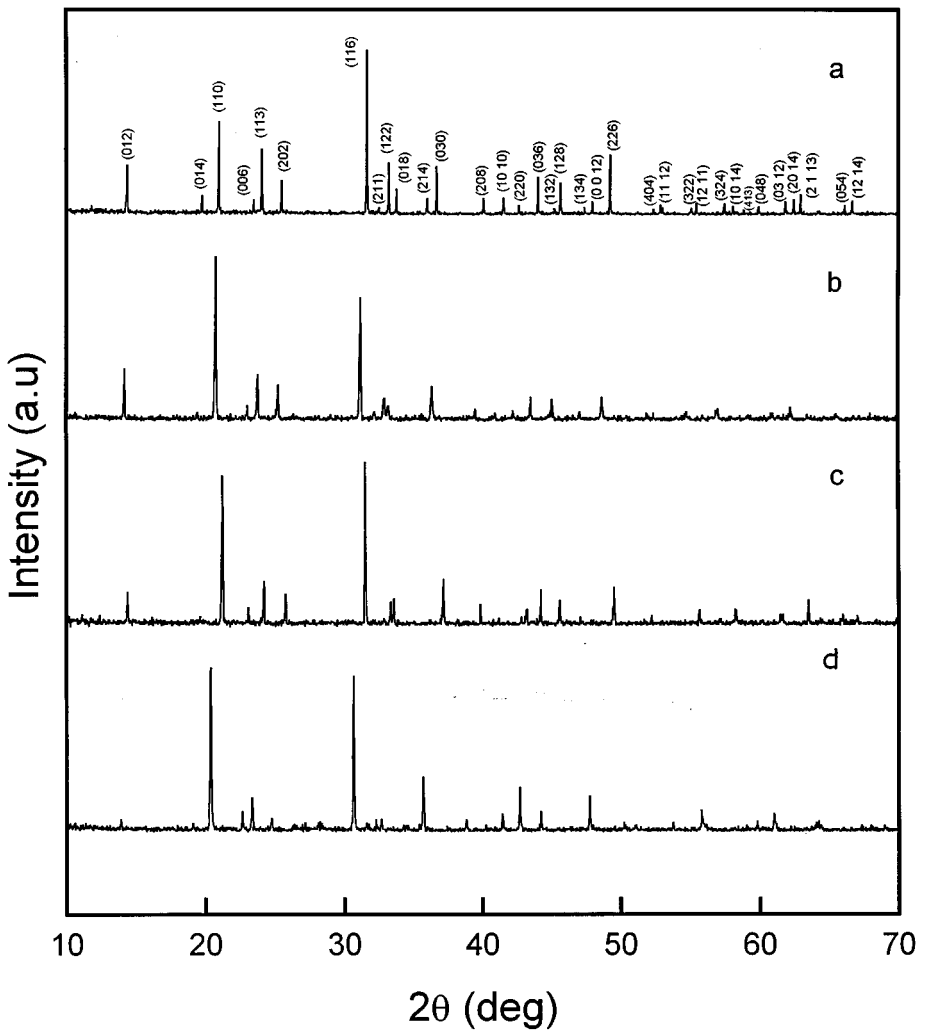

FIG. 1. Powder X-ray diffraction patterns of (a) $PbTi^{3+}Ti^{4+}P_3O_{12}$; (b) $PbCrZrP_3O_{12}$; (c) $PbFeSnP_3O_{12}$; (d) $PbInHfP_3O_{12}$.

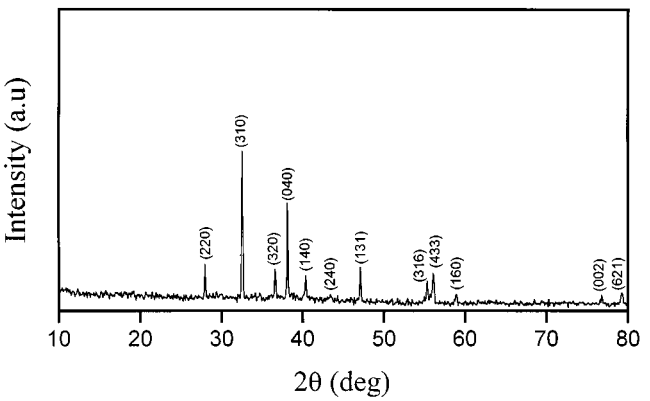

FIG. 2. Powder X-ray diffraction pattern of $Pb_{0.5}Mo_2P_3O_{12}$.

structure. The study does not show the existence of a super structure. This implies that substituted M^{3+} ions should be statistically distributed over the 12*c* (Zr-site in $NaZr_2P_3O_{12}$) octahedral site. To illustrate this, structural analysis of a select compound $PbFeZrP_3O_{12}$ was carried out.

Structure Refinement of $PbFeZrP_3O_{12}$

The room temperature neutron diffraction data were refined by the Rietveld method (21) using the FULLPROF profile refinement program and the peak shape was assumed to be pseudo-Voigt function. The refinement was performed in the space group $R\bar{3}C$. The structure was modeled by assuming that the title compound is isostructural with $NaZr_2P_3O_{12}$. It was assumed that Pb^{2+} occupies the Na site (6*b*), and the Fe/Zr atoms are considered to be statistically distributed over the same crystallographic positions (12*c*). The P atoms are fixed on the 18*e* site and the O atoms are uniformly distributed over two equivalent 36*f* positions. The atom positions of $NaZr_2P_3O_{12}$ were used as the starting model.

In the initial stages of the refinement the scale factor, the instrumental zero point correction, the background parameters, the unit cell parameters, the FWHM parameters, the overall thermal parameters, and the asymmetry factor were refined. After reaching the minimum agreement factors, the structural parameters were refined. The final agreement factors reached are:

$$R_{wp} = 5.03; \quad R_p = 3.95; \quad R_{Bragg} = 5.32$$

$$R_{ex} = 2.44; \quad \chi^2 = 4.25; \quad R_F = 3.80$$

The final hexagonal lattice parameters obtained are $a = 8.6281(3)$ Å and $c = 23.2546(8)$ Å. The parameters are in good agreement with the values obtained from least square fitting. The observed, calculated, and difference patterns obtained from the final refinement are shown in Fig. 3. The atomic coordinates with standard deviations are given in Table 2. Selected bond distances and bond angles are given in Table 3.

Description of the Structure

The proposed structure for the compound $PbFeZrP_3O_{12}$ consists of a framework of two nonequivalent MO_6 octahedra (M = Fe/Zr) and PO_4 tetrahedra sharing their corners. The PO_4 tetrahedra are made up of P–O bonds varying in length between 1.519(2) and 1.532(2) Å. The O–P–O bond angles range from 107.0(1) to 113.6(2). These bond lengths and bond angles are comparable to the reported values of other related phosphate compounds such as $KGe_2P_3O_{12}$ (22), $NaTiSnP_3O_{12}$, (23) and $MoAlP_2O_9$ (24).

The coordination around Fe/Zr can be described as distorted octahedra. The average Fe/Zr–O_1 bond distance is 1.993(3) Å and the Fe/Zr–O_2 bond distance is 2.075(2) Å. Similar bond lengths are found in other compounds of iron with distorted FeO_6 octahedra such as α-Fe_2O_3 where the distances are 1.91 and 2.06 Å (25) and in $KBaFe_2P_3O_{12}$ (26) where one of the FeO_6 octahedra is distorted and has Fe–O bond lengths 1.964 and 2.014 Å. The Zr–O_1 and Zr–O_2 distances are in the range of zirconium–oxygen bond lengths encountered in $NaZr_2P_3O_{12}$ (9), $KZr_2P_3O_{12}$ (27), $Na_5ZrP_3O_{12}$ (28), and $BaZrO_3$ (29) where zirconium has six-fold coordination.

The Pb^{2+} ions located in the type I site are surrounded by six nearest oxygen atoms at a distance 2.650(2) Å. The absence of monoclinic distortion also confirms the occupancy of Pb^{2+} ion at the type I site. The octahedral environment of Pb^{2+} is highly distorted as in the case of NaO_6 octahedra in $NaZr_2P_3O_{12}$ with the bond angles 61.4 and 118.6. The Pb–O bond distance is in the range of values reported for other oxides of lead (where Pb is in a $+2$ oxidation state and has six-fold coordination) such as Pb_2O_3 (30) and $PbSb_2O_6$ (31). In red PbO, lead is surrounded by four oxygen atoms with an interatomic distance of 2.30 (Å) (32), while in $PbTiO_3$ the average Pb–O distance is 2.81 (Å) (12-fold coordination) (33).

Size Effect of Framework M^{3+} and M^{4+} Ions

In the NZP structure, for a series of compounds with a given ion in the type I site the lattice parameter variation is governed by the size of the metal ion of MO_6 octahedra. Figures 4 and 5 show the plots of the hexagonal *a* and *c* parameters of $Pb^{2+}M^{3+}M^{4+}P_3O_{12}$ compounds as a function of the ionic radius (34) of the octahedral site M^{3+} and M^{4+} cations, respectively. For the purpose of comparison, the data for the compounds $PbCrTiP_3O_{12}$ and

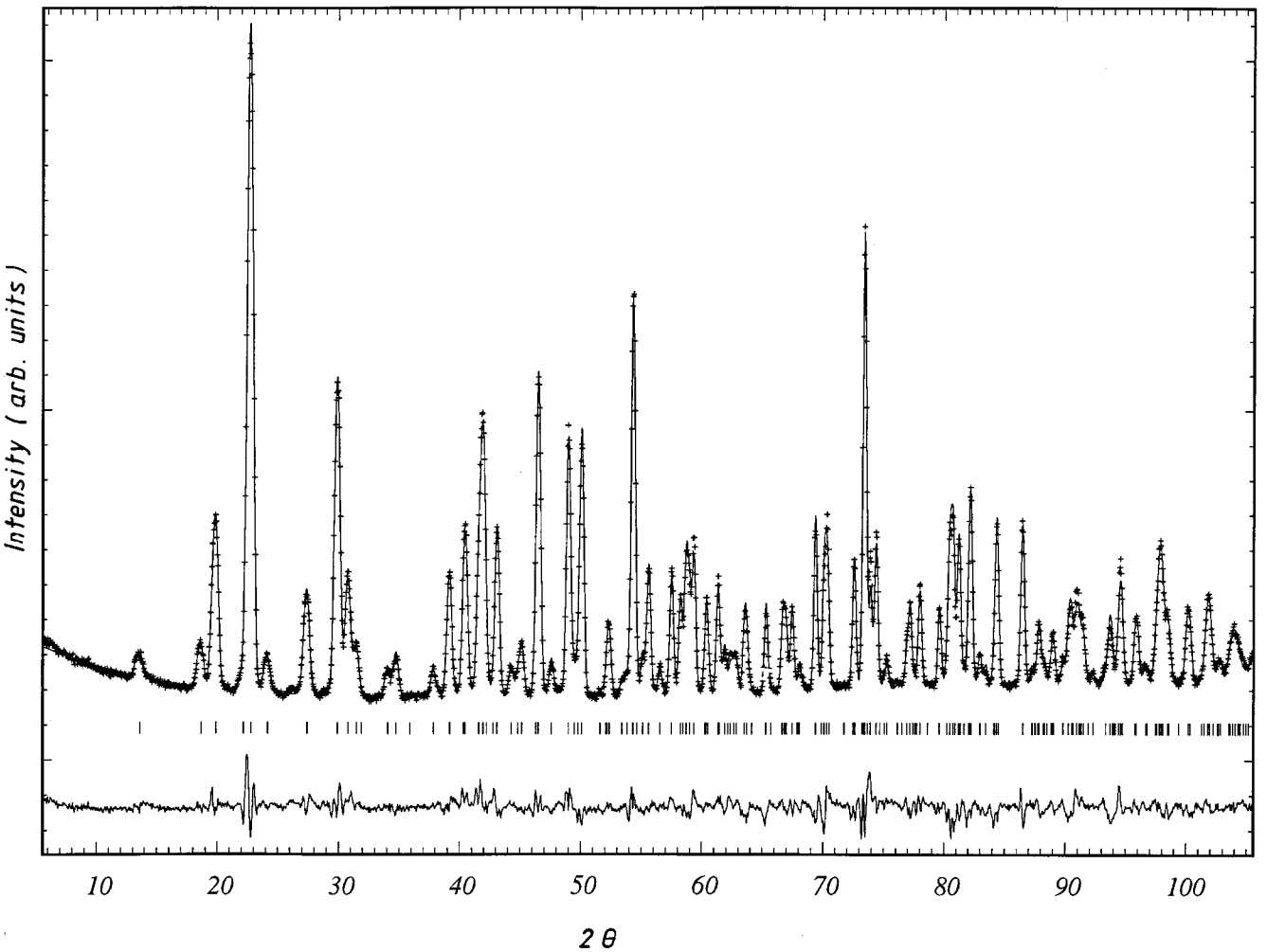

FIG. 3. Observed, calculated and difference profiles of $PbFeZrP_3O_{12}$.

$PbFeTiP_3O_{12}$ (35, 36) are included. Both *a* and *c* parameters show an increase with increasing ionic radius of the M^{3+} cation. This trend is in contrast to the lattice parameter variation when the *A*-site cation size is varied (19). Increase in the ionic radius of the *A*-site cation increases the *c*-parameter and decreases the *a*-parameter.

An increase in the ionic radius of the M^{4+} cation leads to an increase in the *c*-lattice parameter. On the other hand, the *a*-parameter for tin-containing compounds is closer to that of the titanium-containing compounds in spite of the proximity between the radii of the Sn^{4+} ion and the

TABLE 2
Atomic Positions of $PbFeZrP_3O_{12}$

Atom	*x*	*y*	*z*
Pb	0	0	0
Fe	0	0	0.1508(1)
Zr	0	0	0.1508(1)
P	0.2897(3)	0	0.25
O1	0.1762(2)	− 0.0340(3)	0.1965(1)
O2	0.1918(2)	0.1682(2)	0.0920(1)

TABLE 3
Selected Interatomic Distances (Å) and Bond Angles (°)

Bond distances			Bond angles		
6(Pb–O_1)	3.534(3)	O_1–Fe/Zr–O_1	94.2(1)	O_1–P–O_1	113.6(2)
6(Pb–O_2)	2.650(2)	O_1–Fe/Zr–O_2	170.9(1)	O_1–P–O_2	110.1(1)
3(Fe/Zr–O_1)	1.993(3)	O_2–Fe/Zr–O_2	81.4(1)	O_2–P–O_2	109.4(2)
3(Fe/Zr–O_2)	2.075(2)	O_1–Fe/Zr–O_2	93.1(1)	O_2–P–O_1	107.0(1)
2(P–O_1)	1.519(2)	O_1–Fe/Zr–O_2	90.7(1)		
2(P–O_2)	1.532(2)			Pb–O_2–O_2	118.6(1)
				Pb–O_2O_2	61.4(1)

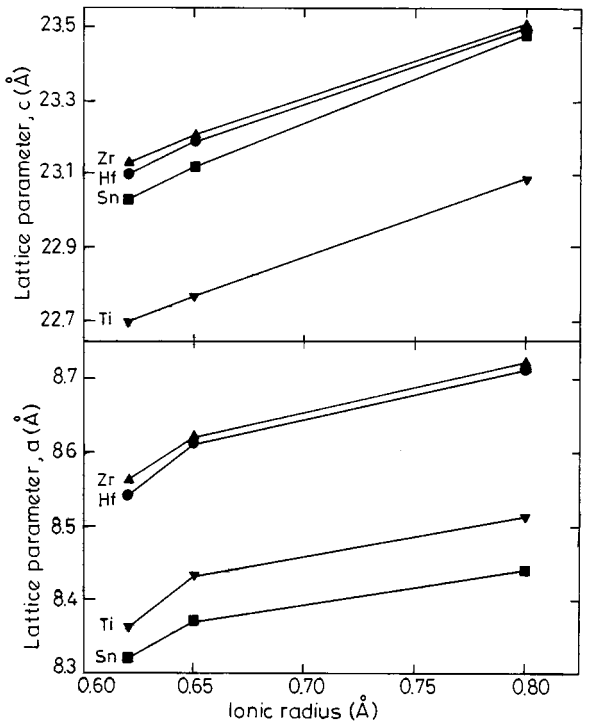

FIG. 4. Variation in the lattice parameters of $PbM^{3+}M^{4+}P_3O_{12}$ with the radii of the M^{3+} (Cr, Fe, and In) cations.

shifted to higher frequency values. This could be due to the presence of Pb^{2+} in the type I site and the polarizing nature of M^{3+}/M^{4+} ions. A shift of about 40 to 60 cm^{-1} toward higher energy is observed in all tin-containing compounds in comparison to the titanium-, zirconium-, and hafnium-containing compounds. A similar observation was made in the case of $CuSn_2(PO_4)_3$ and $AgSn_2(PO_4)_3$ (41). This could be attributed to the weak O–Sn–O bonds due to the filled shell (d^{10}) configuration of Sn^{4+} as proposed by Rodrigo *et al.* (37). This could result in an increase in the covalency of the P–O bond, thereby shifting the frequency of the ν_3 band to higher values. As seen from Fig. 5, the unit cell dimensions also show differences when Sn, the main group element, is introduced into the lattice. The titanium-containing compounds display more resolved spectra. This indicates the presence of highly distorted TiO_6 octahedra. The more polarizing Ti^{4+} ion makes the TiO_6 octahedron more rigid which in turn reduces the symmetry of the PO_4 tetrahedron in comparison to the ions viz., Zr^{4+}, Hf^{4+}, and Sn^{4+}. Apart from the region of the ν_3 band, the ν_1 and ν_4 (symmetric stretching and antisymmetric bending) vibrations occur almost in the same region (~950, 630–643, and 550 cm^{-1}, respectively). The symmetric bending vibrations (ν_2) show a shift of 10–15 cm^{-1} toward a higher energy in all chromium-containing compounds. Hence, the changes in the infrared spectra of all these compounds can be viewed as the

Zr^{4+}/Hf^{4+} ions. Similar behavior was observed in the $NaM_2P_3O_{12}$ (M = Ti, Zr, and Sn) series (37) and in the $NbMP_3O_{12}$ (M = Ti, Zr, Hf, and Sn) series of compounds (38). The anomalous behavior of the Sn^{4+}-containing phases in comparison to that of the other transition metal ion (Ti^{4+}, Zr^{4+}, and Hf^{4+})-containing phases could be attributed to the different nature of the electronic configuration of the tetravalent metal ion as proposed by Rodrigo *et al.* (37).

SPECTROSCOPIC ANALYSIS

Infrared Spectra

Table 4 lists the IR spectral assignments for all the compounds in the range 1700–400 cm^{-1}. Infrared spectra of select compounds are shown in Fig. 6. The compounds show characteristic PO_4 vibrations of the NZP framework (39, 40). The broadbands and the complexity of the spectra indicate that the symmetry of the phosphate group has been reduced to the site symmetry C_2 inside the space group D_{3d} (40). Since the compounds are isostructural, the spectra are similar. However, distinguishable changes are observed in the position of the ν_3 band (antisymmetric P–O stretching mode). As shown in Table 4, the ν_3 band which is observed at 1000 cm^{-1} in the parent phase $NaZr_2P_3O_{12}$ (19) is

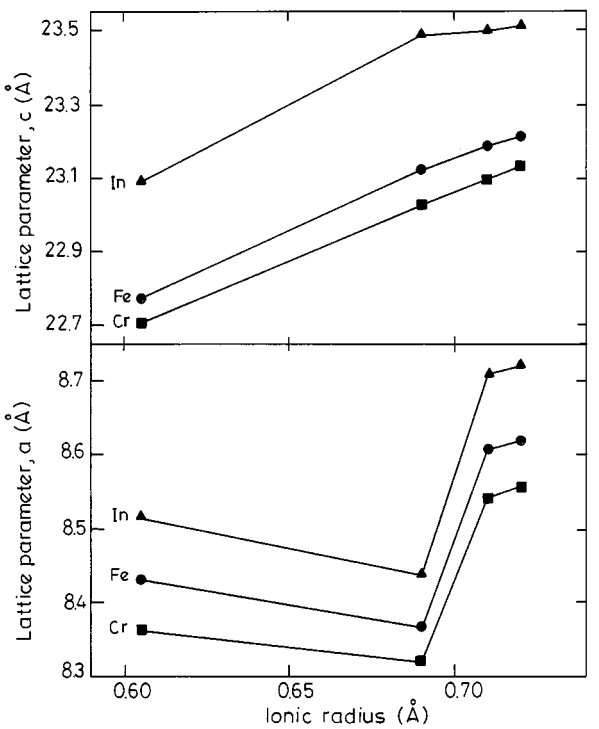

FIG. 5. Variation in the lattice parameters of $PbM^{3+}M^{4+}P_3O_{12}$ with the radii of the M^{4+}(Ti, Sn, Hf, and Zr) cations.

TABLE 4
Assignment (cm^{-1}) of IR Bands for $PbM^{3+}M^{4+}P_3O_{12}$ Compounds

Compound	ν_3 ν_{as} (P–O)	ν_1 ν_s (P–O)	ν_4 δ (P–O)	ν_2 (P–O)
$PbTi^{3+}Ti^{4+}P_3O_{12}$	1193*m*, 1042*sh*, 1009*m*	945m	636*s*, 556*s*	424*m*
$PbCrTiP_3O_{12}$	1203*m*, 1050*sh*, 1001*m*	939sh	659*w*, 635*s*, 552*s*	439*m*
$PbFeTiP_3O_{12}$	1206*m*, 1080*sh*, 1043*sh*, 1001*m*	942sh	631*s*, 546*s*, 580*w*	423*m*
$PbInTiP_3O_{12}$	1210*w*, 1050*sh*, 999*m*	945w	627*s*, 551*s*	429*s*
$PbCrSnP_3O_{12}$	1205*m*, 1062*m*, 1005*sh*	—	632*s*, 553*s*	442*m*
$PbFeSnP_3O_{12}$	1202*b*, 1057*m*	940sh	629*s*, 549*s*	432*m*
$PbInSnP_3O_{12}$	1201*m*, 1065*m*	980sh	627*s*, 556*s*	436*b*
$PbCrHfP_3O_{12}$	1205*m*, 1022*b*	950sh	643*s*, 552*s*	431*w*
$PbFeHfP_3O_{12}$	1200*m*, 1036*m*	965sh	639*s*, 547*s*	424*m*
$PbInHfP_3O_{12}$	1202*m*, 1028*m*	—	637*s*, 547*s*	422*w*
$PbCrZrP_3O_{12}$	1206*m*, 1017*b*	—	637*s*, 548*s*	432*m*
$PbFeZrP_3O_{12}$	1199*m*, 1024*m*	—	637*s*, 542*s*	422*s*
$PbInZrP_3O_{12}$	1199*m*, 1107*sh*, 1057*sh*, 1022*m*	—	633*s*, 544*s*	422*m*

Note. *s*, sharp; *m*, medium; *w*, weak; *b*, broad; and sh, shoulder.

manifestations of the combined effect of the interstitial Pb^{2+} cation and the framework Ti^{4+}, Zr^{4+}, Hf^{4+}, and Sn^{4+} cations on the P–O bonds.

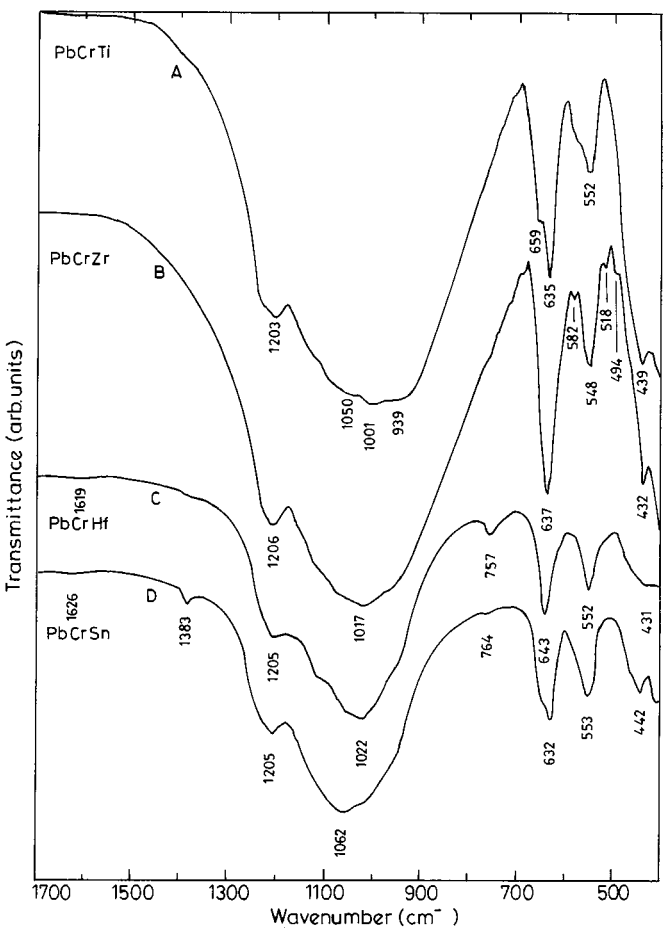

FIG. 6. Infrared spectra of (a) $PbCrTiP_3O_{12}$, (b) $PbCrZrP_3O_{12}$, (c) $PbCrHfP_3O_{12}$, (d) $PbCrSnP_3O_{12}$.

Electronic Spectra

The diffuse reflectance spectra were recorded for chromium- and iron-containing compounds in the range 2000–200 nm. The observed band maxima along with the interelectronic repulsion parameter (B) and the nephelauxetic ratio (β) are given in Table 5. The bands correspond to allowed transitions for Cr^{3+} present in octahedral coordination (42). The values of B and β for the chromium-containing phases are large compared to the values for Cr_2O_3. This indicates that in these compounds, the Cr–O bond is less covalent. In the case of Fe^{3+} the transitions are spin forbidden and hence weak bands are observed (43). The assignments are given in Table 5.

CONCLUSION

It has been shown that the $NaZr_2P_3O_{12}$-type structure is stable toward the substitution of bulky Pb^{2+} ion at the Na

TABLE 5
Assignment of Bands Observed in the Electronic Spectra

Compound	Band maxima (cm^{-1})			B	β
$PbCrTiP_3O_{12}$	18,116[a]	24,096[b]	—	568.3	0.62
$PbCrZrP_3O_{12}$	17,606[a]	25,316[b]	—	797.9	0.87
$PbCrHfP_3O_{12}$	17,857[a]	25,641[b]	—	803.9	0.88
$PbCrSnP_3O_{12}$	17,857[a]	25,773[b]	—	823.6	0.90
$PbFeTiP_3O_{12}$	23,810[c]	21,053[d]	16,528[e]	—	—
$PbFeZrP_3O_{12}$	24,096[c]	20,618[d]	16,393[e]	—	—
$PbFeHfP_3O_{12}$	23,810[c]	20,408[d]	16,806[e]	—	—
$PbFeSnP_3O_{12}$	24,570[c]	21,368[d]	16,367[e]	—	—

[a] $^4A_{2g} \leftarrow {}^4T_{2g}$.
[b] $^4A_{2g} \leftarrow {}^4T_{1g}$ (P).
[c] $^6A_{1g} \leftarrow {}^4E_g$.
[d] $^6A_{1g} \leftarrow {}^4T_{1g}$.
[e] $^6A_{1g} \leftarrow {}^4E_g + {}^4A_{1g}$.

site with a variety of M^{3+} and M^{4+} ions at the Zr site. Structural analysis of the compound $PbFeZrP_3O_{12}$ shows the statistical distribution of Fe^{3+} and Zr^{4+} in the octahedral sites (12*c*). Molybdenum with lower oxidation state is stabilized as $Pb_{0.5}Mo_2P_3O_{12}$.

ACKNOWLEDGMENT

We thank Prof. S. K. Mallik for help in obtaining neutron diffraction data.

REFERENCES

1. J. B. Goodenough, H. Y-P. Hong, and J. A. Kafalas, *Mater. Res. Bull.* **11,** 203 (1976).
2. J. Alamo and R. Roy, *J. Mater. Sci.* **21,** 444 (1986).
3. C. Delmas, P. Cherkaoui, A. Nadiri, and P. Hagenmuller, *Mater. Res. Bull.* **22,** 631 (1987).
4. C. Delmas, A. Nadiri, and J. Soubeyroux, *Solid State Ionics* **28–30,** 419 (1988).
5. U. V. Varadaraju, K. A. Thomas, B. Sivasankar, and G. V. Subbarao, *J. Chem. Soc. Chem. Commun.* **11,** 814 (1987).
6. J Gopalakrishnan and K. Kasturirangan, *Chem. Mater.* **4,** 745 (1992).
7. N. Hirose and J. Kuwano, *J. Mater. Chem.* **4,** 9 (1994).
8. R. Roy, E. R. Vance, and J. Alamo, *Mater. Res. Bull.* **17,** 585 (1982).
9. L. Hagman and P. Kierkegaard, *Acta. Chem. Scand.* **22,** 1822 (1968).
10. R. Masse, A. Durif, J. Cluade-Guitel, and I. Tordjman, *Bull. Soc. Fr. Miner. Cristallogr.* **95,** 47 (1972).
11. A Clearfield, B. D. Roberts, and M. A. Subramanian, *Mater. Res. Bull.* **19,** 219 (1984).
12. B. Matkovic, B. Prodic, and M. Sljukic, *Bull. Soc. Chim. Fr.* 1777 (1968).
13. R. Masse, *Bull. Soc. Fr. Miner. Cristallogr.* **93,** 500 (1970).
14. S. Senbhagaraman and A. M. Umarji, *J. Solid State Chem.* **85,** 169 (1990).
15. J. Alamo and R. Roy, *J. Amer. Ceram. Soc.* **63,** C78–80 (1984).
16. G. V. Subba Rao, U. V. Varadaraju, K. A. Thomas, and B. Sivasankar. *J. Solid State Chem.* **70,** 101 (1987).
17. A. Leclaire, M. M. Borel, A. Grandin, and B. Raveau, *Acta Crystallogr. Sect. C* **45,** 699 (1989).
18. A. Leclaire, J. C. Monier, and B. Raveau, *J. Solid State Chem.* **59,** 301 (1985).
19. M. Sugantha, U. V. Varadaraju, and G. V. Subba Rao, *J. Solid State Chem.* **111,** 33 (1994).
20. A. Leclaire, J. Chardon, A. Grandin, M. M. Borel, and B. Raveau, *J. Solid State Chem.* **108,** 291 (1994).
21. H. M. Rietveld, *Acta Crystallogr.* **2,** 65 (1969).
22. R. Brochu, M. Louer, M. Alami, M. Alqaraoui, and D. Louer, *Mater. Res. Bull.* **32,** 113 (1997).
23. M. P. Carrosco, M. C. Guillem, and J. Alamo, *Mater. Res. Bull.* **27,** 603 (1992).
24. A. Leclaire, M. M. Borel, A. Grandin, and B. Raveau, *Z. Kristallogr.* **190,** 135 (1990).
25. R. W. G. Wyckoff, "Crystal Structures," 2nd ed., Vol. 2, p. 7. Wiley, New York, 1964.
26. P. D. Battle, A. K. Cheetham, W. T. A. Harrison, and G. J. Long, *J. Solid State Chem.* **62,** 16 (1986).
27. M. Sljukic, B. Matkovic, B. Prodic, and D. Anderson, *Z. Kristallogr.* **130,** 148 (1969).
28. J. P. Boilot, G. Collin, and R. Comes, *J. Solid State Chem.* **50,** 91 (1983).
29. A. Clearfield and P. A. Vaughan, *Acta Crystallogr.* **9,** 555 (1956).
30. J. Bouvaist and D. Weigel, *Acta Crystallogr. A* **26,** 501 (1970).
31. A. J. C. Wilson, "Structure Reports," Vol 8, p. 156. N. V. A. Oosthoek's Uitgevers Mij, Utrecht, 1941.
32. J. Leciejewicz, *Acta Crystallogr.* **14,** 1304 (1961).
33. G. Shirane, R. Pepinsky, and B. C. Frazer, *Acta Crystallogr.* **9,** 131 (1956).
34. R. D. Shananon, *Acta Crystallogr. A* **32,** 751 (1976).
35. P. Rene and B. Abdelhamid, *Bull. Soc. Fr. Miner. Cristallogr.* **100,** 5 (1977).
36. B. Abdelhamid and P. Rene, *Bull. Soc. Fr. Miner. Cristallogr.* **99,** 254 (1976).
37. J. L. Rodrigo and J. Alamo, *Mater. Res. Bull.* **26,** 475 (1991).
38. K. V. Govindan Kutty, R. Asuvathraman, C. K. Mathews, and U. V. Varadaraju, *Mater. Res. Bull.* **29,** 1009 (1994).
39. M. Barj, H. Perthuis, and Ph. Colomban, *Solid State Ionics* **11,** 157 (1983).
40. A. Mbandza, E. Bordes, and P. Courtine, *Mater. Res. Bull.* **20,** 251 (1985).
41. J-M. Winand, A. Rulmont, and P. Tarte, *J. Solid State Chem.* **107,** 356 (1993).
42. L. E. Orgel, *J. Chem. Phys.* **23,** 1004 (1955).
43. N. F. Ried, H. K. Perkins, and M. J. Sienko, *Inorg. Chem.* **7,** 119 (1968).